Equilibrium polymerization of cyclic carbonate oligomers. III. Chain branching and the gel transition

P. Ballone
Institut für Festkörperforschung, Forschungszentrum Jülich, D-52425 Jülich, Germany
and Università degli Studi di Messina, Dipartimento di Fisica, Contrada Papardo, I-98166 Messina, Italy

R. O. Jones[a)]
Institut für Festkörperforschung, Forschungszentrum Jülich, D-52425 Jülich, Germany

(Received 24 April 2002; accepted 12 July 2002)

Ring-opening polymerization of cyclic polycarbonate oligomers, where monofunctional active sites act on difunctional monomers to produce an equilibrium distribution of rings and chains, leads to a ''living polymer.'' Monte Carlo simulations [two-dimensional (2D) and three-dimensional (3D)] of the effects of single [J. Chem. Phys. **115**, 3895 (2001)] and multiple active sites [J. Chem. Phys. **116**, 7724 (2002)] are extended here to trifunctional active sites that lead to branching. Low concentrations of trifunctional particles c_3 reduce the degree of polymerization significantly in 2D, and higher concentrations (up to 32%) lead to further large changes in the phase diagram. Gel formation is observed at high total density and sizable c_3 as a continuous transition similar to percolation. Polymer and gel are much more stable in 3D than in 2D, and both the total density and the value of c_3 required to produce high molecular weight aggregates are reduced significantly. The degree of polymerization in high-density 3D systems is increased by the addition of trifunctional monomers and reduced slightly at low densities and low c_3. The presence of branching makes equilibrium states more sensitive (in 2D and 3D) to changes in temperature T. The stabilities of polymer and gel are enhanced by increasing T, and—for sufficiently high values of c_3—there is a reversible polymer–gel transformation at a density-dependent floor temperature.
 [DOI: 10.1063/1.1505023]

I. INTRODUCTION

Many common industrial polymers [polyethylene (PE), polyvinyl chloride (PVC), polystyrene (PS), etc.] comprise chains of difunctional monomers that are topologically one-dimensional,[1] a feature shared by important biological molecules such as polysaccharides, proteins, RNA, and DNA.[2] The addition of multifunctional units can lead to nonlinear structures (branching, star polymers, combs, networks, etc.) differing in the nature of the branching centers, their ordered or statistical distributions, and the presence of primary and secondary (grafted) chains, etc. Multifunctional units can arise as additives, impurities, or from parasitic reactions,[3] and the resulting crosslinks can alter greatly the polymer size distribution and the dynamical (e.g., diffusion, viscosity) and mechanical properties.[4,5] Moreover, branching can result in transitions to qualitatively new phases such as gels and rubber.[6] The distribution of multifunctional units depends mainly on statistical properties (entropy) at low concentrations, while potential energy changes, steric effects, and stoichiometry are important at high concentration. Kinetic effects are important, since the formation and breaking of covalent bonds often involve large energy barriers and a suitable catalyst, whose nature and concentration could affect the number and distribution of branching points.

Most investigations of polymer branching and gelation have been devoted to systems in which chemical bonds form suddenly and irreversibly, leading to nonequilibrium conditions.[7] However, real systems often show reversibility, and equilibrium considerations are crucial in the polymerization and gelation stages. The complexity of polymers and the low concentration of branching centers often prevent their experimental investigation, so that computer simulations assuming thermodynamic equilibrium[8,9] and the presence of multifunctional units provide an attractive alternative. In spite of rapid progress,[10] however, simulations of equilibrium polymers cannot yet explore all relevant systems and conditions, and very few have included branching.[11]

We study branching by extending a model[12,13] of the ring-opening polymerization (ROP) of cyclic carbonate oligomers activated by a metallo-organic catalyst.[14] Monomers are represented by Lennard-Jones (LJ) particles that move on the continuum and form one (chain terminations) or two (regular monomers) bonds with other particles. Chain terminations can be *active* (catalyst heads) or *inert* (such as phenol chain terminations). The number of bonds is fixed for each particle, but pairs of bonds can be interchanged if one of the particles is active. This model excludes branching and is characterized by the equilibrium between a polymer at high density and a low-density unpolymerized phase. The details of the thermodynamic, structural, and dynamical properties depend on the temperature T and the concentration c_a of active particles.

We extend the model here by introducing LJ particles

a)Author to whom correspondence should be addressed. Electronic mail: r.jones@fz-juelich.de

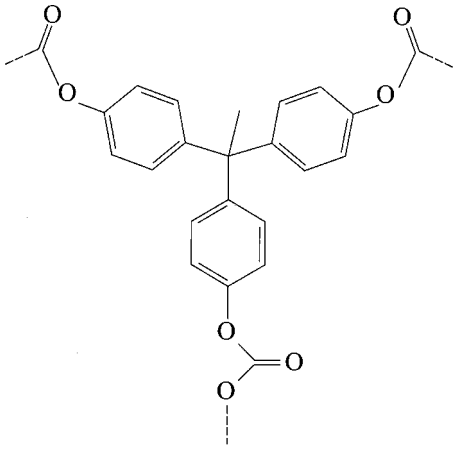

FIG. 1. Schematic view of the branching center in bisphenol-A polycarbonate produced by the ring-opening polymerization of cyclic oligomers in the presence of small amounts of 1,1,1-*tris*(4-hydroxyphenyl)ethane, THPE. See Ref. 5.

that form three bonds and lead to branching, and Fig. 1 shows an example in the polycarbonate context.[5] This is the product of a reaction whose course depends on density, T, and the concentration of additives and impurities, and the resultant polymer shows a shear sensitivity that is directly related to the amount of branching agent and inversely related to the amount of the initiator. As in our previous work,[12,13] a low concentration c_a of active particles allows equilibration with respect to the bond configuration. The model emphasizes the role of entropy over potential energy, since all particles interact by the same LJ potential, all bonds are equivalent, and their number is conserved.

We perform simulations in two-dimensional (2D) and three-dimensional (3D) for concentrations of trifunctional units c_3 from 0.1% to 32% and densities covering the polymerization line found for $c_3=0$. The degree of polymerization in 2D samples is reduced for $c_3 \sim 1\%$, leading to compact molecules with open linear segments and closed loops. This trend is reversed at high density and higher c_3 values, because cross-linking of molecular units overcomes the reduction in molecular size. At a value of c_3 that depends on density and T, a molecular aggregate extends over the entire system, and we identify this as the gel transition for our model.

The 3D results are similar, but the enhanced stability of large polymeric aggregates leads to quantitative differences. The polymer phase is stable at lower densities, and the gel transition occurs at either lower density or lower c_3. The addition of trifunctional units at low concentration decreases the degree of polymerization in low density samples, but this effect is weaker than in 2D and is reversed at high density. Gel formation is apparently a continuous phase transformation in both two and three dimensions, showing large fluctuations in the polymer size and a clear similarity to the percolation transition.[6]

Theories of gelation go back to the mean field (MF) work of Flory[15] and Stockmayer.[16] Lattice models[17] beyond MF have been studied,[18,19] and there are recent studies incorporating temperature effects.[20,21] Nevertheless, MF approaches, with some use of Monte Carlo (MC) to incorporate geometrical factors, are widely used to investigate branching and gelation in long-chain polymers,[22] and similar methods have been used to study related highly cross-linked systems.[23] The absence of potential energy models in most studies rules out discussions of temperature effects and thermal equilibration, and this work is among the first to include branching in the simulation of equilibrium polymerization based on a continuum model of particle interactions. Branching arising from free-radical polymerization has been investigated recently by MC simulations for a continuum model with an explicit potential energy function.[11] This work makes contact with ours, in spite of differences in detail and in the polymerization mechanism assumed.

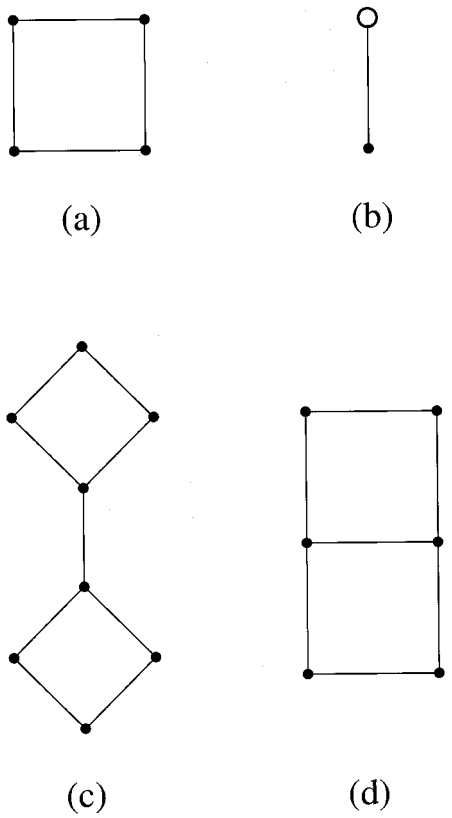

FIG. 2. Schematic structure of oligomers present at the beginning of the simulation. The large empty circle identifies an active chain termination. Inert chain terminations, difunctional, and trifunctional monomers are represented by a solid dot.

II. THE MODEL AND THE COMPUTATIONAL METHOD

Our model generalizes one used to study the equilibrium ring-opening polymerization (ROP) of cyclic carbonate oligomers by a catalyst.[12] The initial oligomers are cyclic tetramers of bisphenol A polycarbonate (BPA-PC) [Fig. 2(a)], and the catalyst (e.g., an alkali-substituted phenol) is represented by a dimer with one active and one inert termination [Fig. 2(b)]. Monomers (LJ particles) move on the continuum in either 2D or 3D, and are joined by harmonic springs (covalent bonds in the polymer backbone), so that the potential energy of a collection of $(N/4)$ cyclic tetramers, for example, is

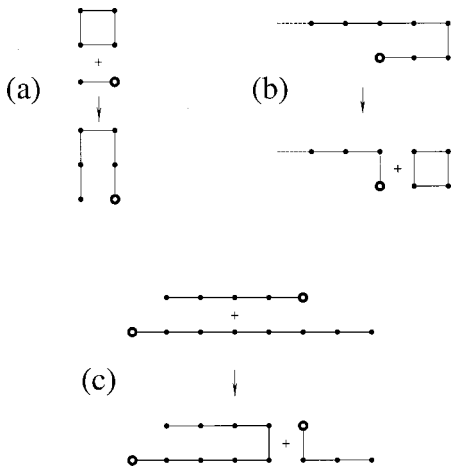

FIG. 3. Elementary bond-interchange mechanisms.

$$V(\mathbf{r_1},\ldots,\mathbf{r_N}) = \epsilon \sum_{i>j}^{N'} \left\{ \left(\frac{\sigma}{|\mathbf{r}_i - \mathbf{r}_j|} \right)^{12} - \left(\frac{\sigma}{|\mathbf{r}_i - \mathbf{r}_j|} \right)^{6} \right\} + \frac{1}{2} k \sum_{\alpha=1}^{(N/4)} \{ (\mathbf{r}_{4\alpha-3} - \mathbf{r}_{4\alpha})^2 + (\mathbf{r}_{4\alpha-3} - \mathbf{r}_{4\alpha-2})^2 + (\mathbf{r}_{4\alpha-2} - \mathbf{r}_{4\alpha-1})^2 + (\mathbf{r}_{4\alpha-1} - \mathbf{r}_{4\alpha})^2 \}. \quad (1)$$

The prime on the first sum indicates that the LJ interaction is absent when i and j are connected by the harmonic potential. The attractive LJ interaction of monomers corresponds to a poor-solvent condition, and the assumption that particle pairs form only single bonds reflects the chemistry of polycarbonates. The units of length and energy are σ and ϵ, respectively, and the density is described by the packing fraction η ($\eta = \pi\rho\sigma^2/4$ in 2D, $\eta = \pi\rho\sigma^3/6$ in 3D). Very floppy molecules result from our choice of k ($k = 3\epsilon$) and allow an efficient sampling of intra- and intermolecular degrees of freedom. The polymers are fully flexible, since we neglect angle bending and torsion contributions.

The generalization to polymer branching considers tetramer pairs joined by one additional bond [Fig. 2(c)]. For $c_3 > 25\%$ we add rectangular hexamers [Fig. 2(d)]. Density functional studies of the basic ROP step[24] have shown that the active termination lowers the free energy barrier for the interchange of bond pairs, allowing bonding patterns to change while conserving both the total number of bonds and the number connecting each particle. The basic mechanisms leading to equilibrium polymerization (Fig. 3) are the same for all particles, irrespective of the number of bonds (one, two, or three) they form.

All simulations start from well equilibrated mixtures of isolated [Fig. 2(a)] and fused tetramers [Fig. 2(c)] corresponding to a given concentration c_3 of trifunctional units. After equilibration, all samples contain $N = N_2 + N_3 = 10^4$ particles, with N_2 difunctional and N_3 trifunctional units, and $(2N_2 + 3N_3)/2$ bonds. Following Refs. 12 and 13, we introduce N_a active heads ($N_a = 10,16,25,36$) and an equal number of inert chain terminations by adding N_a linear dimers [Fig. 2(b)] at random positions. The concentrations of catalyst particles ($0.1\% < c_a < 0.36\%$) are similar to those used in industrial practice.

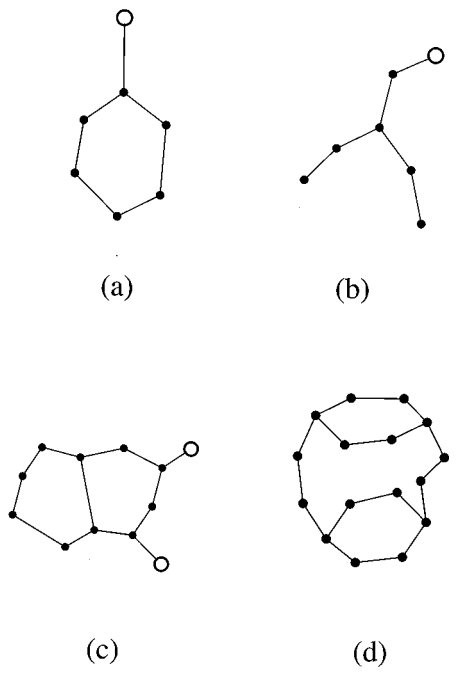

FIG. 4. Schematic view of molecular units containing mono-, di-, and trifunctional monomers. (a) $N_3 = 1$, $N_t = 1$, $N_{\text{loop}} = 1$; (b) $N_3 = 1$, $N_t = 3$, $N_{\text{loop}} = 0$; (c) $N_3 = 4$, $N_t = 2$, $N_{\text{loop}} = 2$; (d) $N_3 = 4$, $N_t = 0$, $N_{\text{loop}} = 3$.

The interaction potentials are the same for all particles, but *active* particles mimic the behavior of the catalytic head in MOPh by (a) forming one and only one bond, and (b) exchanging bonds only when at least one of the bonds involves an active particle. Bond configurations are sampled by attempting a bond interchange every N single particle steps (N is of the order of the number of particles in the system): We select an active particle, identify its nearest neighbor (excluding the particle connected to it by an intramolecular bond), and link this pair and two covalently bonded neighbors as shown in Fig. 3. The interchange conserves the total number of bonds and is accepted or rejected on the basis of the changes in potential energy and T, using the Metropolis algorithm to approach the Boltzmann distribution for the potential energy. The (constant volume) Metropolis MC method is also used to sample the potential energy, where random moves are attempted to translate either single particles or whole molecules with relative probability and steps chosen to achieve an acceptance ratio of ~ 0.5 in both cases.

The bond interchange mechanism implies several topological constraints, e.g., a molecule with a single trifunctional particle must include one [Fig. 4(a)] or three [Fig. 4(b)] chain terminations (either active or inert). In the former case, the molecule contains one closed loop. In general, a molecule with n_3 trifunctional units may contain at most $(n_3 + 2)$ chain terminations, forming $n_{\text{loop}} = (n_3 + 2 - N_t)/2$ closed loops, where $N_t \leqslant (n_3 + 2)$ is the number of chain terminations. These conditions generalize those for systems without branching,[12,13] where only open chains and simple

rings are present, and the number of open chains is constant (half of the total number of chain terminations).

The system is monitored by computing the size distribution and the average size of molecules with one or more chain terminations or at least one trifunctional unit. These populations account for a large fraction of the total mass in the polymeric phase, and the analysis of either provides similar information. The distribution of rings is discussed separately. The degree of polymerization is characterized by the percentage $W_+(L)$ of the total mass in molecules larger than L, irrespective of their composition (mono-, di-, or trifunctional units). $W_+(L)$ is a monotonic function, decreasing from 100% at $L=1$ to 0% at large L values. A higher degree of polymerization corresponds to a more extended tail of $W_+(L)$ in the large L range.

Equilibration involved more than 2×10^5 MC steps/particle in all systems, with an equal number ($>2\times10^5$) of bond interchange attempts, and statistics were accumulated on additional runs of equal length. As described previously,[12] the diffusion (D) and viscosity (s) coefficients were computed by microcanonical molecular dynamics (MD) runs for systems of fixed bonding configuration,[25] starting from atomic positions equilibrated by MC and random velocities selected from a Gaussian distribution. Together with σ and ϵ, the unit mass (the mass of the monomer m) determines the unit of time $\tau=\sigma(m/\epsilon)^{1/2}$. The mass of the polymer M is equal to the number of monomers. The equations of motion were integrated using the velocity Verlet algorithm with a time step of 0.01τ. Equilibration runs lasted 1000τ, and statistics was accumulated over further 3000τ.

III. POLYMERIZATION AND GEL TRANSITION IN 2D

Simulations for 2D systems with $c_3=0$ showed[12,13] that the polymeric phase is stable if $\eta\geqslant0.16$, and a small number of trifunctional units could enhance polymerization by allowing the formation of interchain links and aggregates of chain segments. For 2D systems with $c_3\sim0.1\%-1\%$, however, the addition of trifunctional particles *lowers* the degree of polymerization significantly, as can be seen from the c_3-dependence of the average size $\langle L_l\rangle$ for molecules with at least one chain termination (Fig. 5, $\eta=0.3$, $c_a=0.16\%$, and $T=3$). In the absence of branching, open chains form a large fraction (54%) of the total mass, the average length of open chains exceeds 300 monomers, and the equilibrium size distribution extends up to 2000 monomers.

Molecules with at least one chain termination form a large fraction of the mass in the presence of branching, so that their average length is one measure of the degree of polymerization. Figure 5 shows that, at the density corresponding to $\eta=0.3$, $\langle L_l\rangle$ decreases significantly when a few trifunctional monomers are added, remains below 200 over a wide range of c_3 concentrations, and shows a peak at $c_3=25\%$ (close to the value for $c_3=0$). The nonmonotonic behavior of $\langle L_l\rangle$ (c_3) and the cusp at $c_3=0$ indicate unusual stoichiometric effects, and the relative importance of these two features depends on η (see Fig. 5). The drop of $\langle L_l\rangle$ near to the origin is significant at all densities, but the height (and even the existence) of the peak at $c_3=25\%$ depends strongly on η: at $\eta=0.2$ polymerization is almost suppressed over the range $0.5\leqslant c_3\leqslant32\%$, while at $\eta=0.5$ the peak at $c_3=25\%$ identifies clearly a new (gel) phase quite different from the polymer found for $c_3=0$. This new phase is formed across a phase transition, which, together with the polymerization transition found previously,[12,13] allows us to identify three distinct phases for the model: a fluid phase made of oligomers; a gel, in which most of the mass is included in a single molecule; and a polymeric phase, made by several linear or branched aggregates of fairly large ($L\geqslant100$ monomers) size.

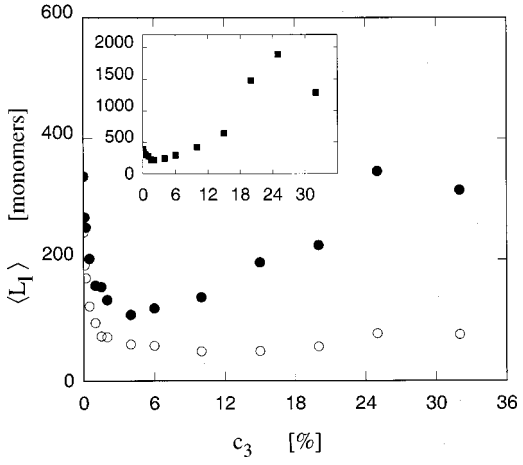

FIG. 5. Average mass of molecules carrying at least one chain termination. Simulations have been performed in 2D at $T=3$. Empty circles: $\eta=0.2$; solid dots: $\eta=0.3$; filled squares (inset): $\eta=0.5$.

The same features appear in Fig. 6, which shows the average size of molecules with at least one trifunctional monomer $\langle L_3\rangle$ (c_3). For small values of c_3, $\langle L_3\rangle$ is nearly equal to $\langle L_l\rangle$ and decreases rapidly with increasing c_3 close to the origin. At all densities, the peak at $c_3=25\%$ is much less pronounced than in the case of $\langle L_l\rangle$. The initial decrease in $\langle L_l\rangle$ and $\langle L_3\rangle$ as c_3 increases is due primarily to the lowering of the degree of polymerization (see Fig. 7). At $\eta=0.3$ and $T=3$, for example, the addition of 1% of trifunctional particles reduces significantly the high L tail of $W_+(L)$. As c_3 increases, $W_+(L)$ recovers its initial width for $c_3\sim10\%$, has a maximum for $c_3=25\%$, and decreases slowly for larger c_3.

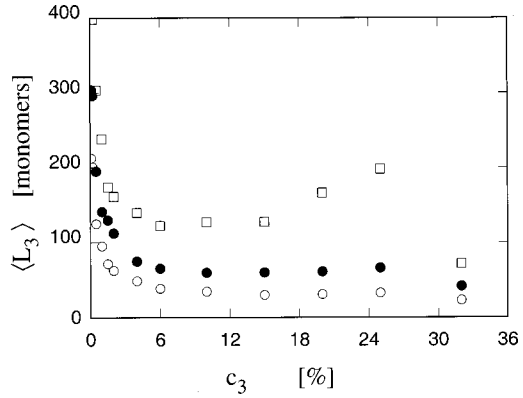

FIG. 6. Average mass of molecules carrying at least one trifunctional monomer. Simulations have been performed in 2D at $T=3$. Empty circles: $\eta=0.2$; solid dots: $\eta=0.3$; empty squares: $\eta=0.5$.

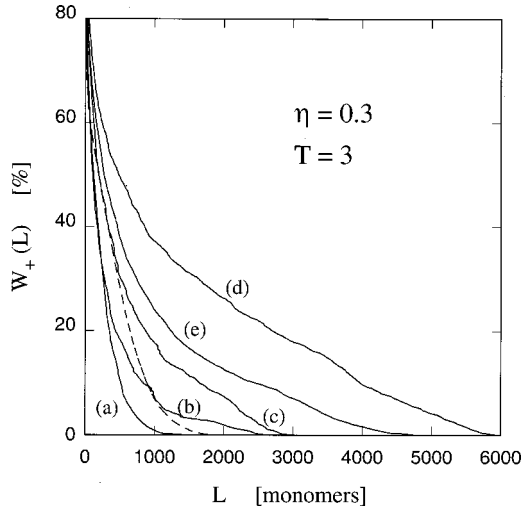

FIG. 7. Percentage W_+ of molecules whose mass exceeds L. The full lines (a), (b), (c), (d), and (e) are for $c_3=1\%$, 10%, 20%, 25%, and 32%, respectively. The dashed line is the result for $c_3=0$.

This behavior parallels the c_3-dependence of $\langle L_l \rangle$ and results from several competing mechanisms. Trifunctional units lead to compact structures (Fig. 8) that decrease the entropy advantage of large molecules (see below). This mechanism is enhanced by the relaxation of the topological rules caused by the presence of trifunctional units, which means that chain and ring combinations can occur, increasing the multiplicity and the entropy of smaller aggregates. Nevertheless, trifunctional monomers may link molecules into larger aggregates, increasing the degree of polymerization and leading to a gel phase.

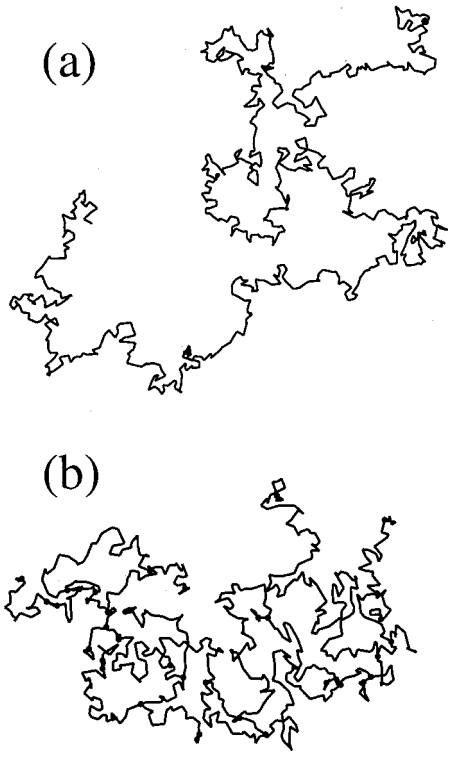

FIG. 8. Typical molecular structures in 2D simulations at $\eta=0.3$, $T=3$, and $c_a=0.16\%$. (a) $c_3=0$; (b) $c_3=4\%$.

As discussed previously,[12,13] polymerization is driven by the entropy advantage of long, open chains over cyclic oligomers. The competing mechanisms of Figs. 3(a) and 3(b) mean that the growth of linear chains from cyclic tetramers is due to the reaction of the active head with a new tetramer, while ring separation is due to the reaction of the head with its own tail. The latter is more probable in compact configurations, which is consistent with the relationship found between molecular shape and the degree of polymerization. This can be quantified by computing the radius of gyration R_g of polymeric molecules,

$$R_g^2=\frac{1}{2L^2}\sum_{i\neq j}^{L}\langle(\mathbf{x_i}-\mathbf{x_j})^2\rangle, \tag{2}$$

where the sum extends over all particles i and j belonging to one molecule of size L. R_g^2 increases as L increases, and—for our potential and thermodynamic conditions—scales approximately as L for all samples and molecular sizes exceeding $L\sim 50$. However, the average values for the samples at $c_3>0\%$ are systematically lower than those for $c_3=0$, and the reduction of R_g^2 is $\sim$50% for molecules with $L\sim 300$, even for $c_3\sim 1\%$. As discussed in Sec. V, the reduction of R_g and the relaxation of topological constraints lead to a substantial increase in the number of closed polymeric loops (rings or loops belonging to more complex molecules) and might contribute to the cusp in $\langle L_l \rangle(c_3)$.

In the presence of long chains or many trifunctional sites, linking molecules to larger aggregates may lead to percolation across the entire system. Although we do not assume the absence of closed loops and steric hindrance, as often made in studies of gelation,[6,26] our results are consistent with a percolative description of this phase transformation. The gel forms via a continuous transition with increasing c_3, resulting from the linking of aggregates with a wide range of sizes. The accompanying anomalous increase of size fluctuations (Table I) supports both the continuous nature of the phase transformation and the connection to percolation.

At fixed (and relatively high) c_3, the gel transition occurs with increasing density, which stabilizes the underlying polymeric phase. The transition remains continuous, but it occurs at densities well above the polymerization line in the absence of branching [$\eta_p(2\mathrm{D})=0.16$] and is much more abrupt than as a function of c_3 (Fig. 9). The difference between the polymer and gel is blurred for the largest values of c_3, since branching and interchain connectivity are already evident at low to medium sizes. As seen from the results for $c_3=25\%$ in Fig. 9, it is difficult to distinguish a polymeric plateau in $\langle L_l \rangle(\eta)$ from the gel phase.

Uncertainties in simulating the gel transition could be reduced by a finite scaling analysis,[27] and the determination of scaling exponents would require far more extensive computations on much larger samples. Here we locate the transition point where the average length $\langle L_l \rangle$ recovers its original ($c_3=0$) value, i.e., where the linking of chain segments overcomes the effect of closed loop formation. For $c_3 \leqslant 32\%$, Fig. 5 shows that the transition does not occur for

TABLE I. Average size fluctuation ($\sqrt{\langle L_l^2\rangle - \langle L_l\rangle^2}$) and relative size fluctuation ($\sqrt{\langle L_l^2\rangle - \langle L_l\rangle^2}/\langle L_l\rangle$, second line, in parentheses) for 2D and 3D systems at different densities and concentrations of trifunctional monomers.

2D	$c_3=0$	$c_3=6\%$	$c_3=10\%$	$c_3=15\%$	$c_3=20\%$	$c_3=25\%$	$c_3=32\%$
$\eta=0.2$	233	70	55	54	77	111	106
	(0.95)	(1.21)	(1.12)	(1.11)	(1.37)	(1.42)	(1.38)
$\eta=0.3$	293	183	223	370	389	744	754
	(0.87)	(1.53)	(1.62)	(1.90)	(1.74)	(2.15)	(2.40)
$\eta=0.5$	353	544	1133	1668	3082	3359	2512
	(0.91)	(1.87)	(2.69)	(2.61)	(2.08)	(2.14)	(2.21)
3D	$c_3=0$	$c_3=0.2\%$	$c_3=0.5\%$	$c_3=1\%$	$c_3=1.5\%$	$c_3=2\%$	$c_3=2.5\%$
$\eta=0.05$	423	528	758	989	1198	1384	1301
	(0.94)	(1.26)	(1.87)	(2.42)	(2.84)	(3.02)	(2.43)

$\eta=0.2$, it is approached at $c_3=25\%$ for $\eta=0.3$, and it occurs at $c_3\sim 10\%$ at $\eta=0.5$. At the optimal stoichiometry $c_3=25\%$, gelation causes a dramatic change of $W_+(L)$ as a function of density (Fig. 10). It is clear that the gel transition in 2D requires a sizable concentration of trifunctional particles.

The molecular size distributions at equilibrium are characterized by the percentages of monomers in a molecule of length L that contain chain terminations and trifunctional particles, $P_l(L)$ and $P_3(L)$. Other studies have used the probability for a molecule to have size L, $C_l(L)$, and $C_3(L)$, which (apart from normalization) are related by $P_l(L)=LC_l(L)$ and $P_3(L)=LC_3(L)$. We use the former to emphasize the role of the (relatively few) large aggregates that represent a sizable fraction of the total mass. Analogous definitions will be used for the probability distributions $P_r(L)$ and $C_r(L)$ for simple rings, and the distribution functions are normalized so that

$$\sum_L P_l(L)=\sum_L P_3(L)=100. \tag{3}$$

The functions $P_l(L)$ and $P_3(L)$ provide equivalent descriptions, and we focus on $P_l(L)$.

Figure 11 shows $P_l(L)$ for samples at $\eta=0.5$, $T=3$, and c_3 values covering the gel transition ($c_3\sim 10\%$ for these conditions). In the absence of branching,[13] $P_l(L)$ is approximated well by the Zimm–Schulz function $\propto L^\gamma \times \exp[-\gamma L/\langle L\rangle]$, with an exponent γ close to the value ($\gamma=43/32$) found in Ref. 28 for a model closely related to the present one. The addition of branching centers affects significantly $P_l(L)$ at low values of c_3, as indicated by the rapid decrease of $\langle L_l\rangle$ close to $c_3=0$: The peak of $P_l(L)$ moves towards lower sizes, while, at the same time, the tail of the distribution extends to higher sizes. As a result, it deviates significantly from the Zimm–Schulz distribution, and an exponential form [$P_l(L)\propto\exp[-\alpha L/\langle L\rangle]$, $\alpha\sim 0.36$] is more appropriate in the c_3 range corresponding to a lower degree of polymerization (see the curve for $c_3=1\%$ in Fig. 11). In the gel phase, $P_l(L)$ shows a bimodal distribution, with the high-L peak centered at sizes ($L\sim 9000$ monomers) close to the total sample size (see the curve for $c_3=25\%$ in Fig. 11). At the gel transition ($c_3=10\%$), $P_l(L)$ is nearly constant over a wide size range, which explains the large fluctuations in $\langle L_l\rangle$.

IV. POLYMERIZATION AND GEL TRANSITION IN 3D

Many features observed in 2D systems are observed in 3D, although the greater stability of the 3D polymer phase influences the properties of branched systems. The reduction of $\langle L_l\rangle$ at low c_3 is apparent in Fig. 12, which shows the dependence on c_3 of $\langle L_l\rangle$ at $T=3$ and density $\eta=0.05$ slightly above the polymerization line [$\eta_p(3D)=0.04$].[13] The rapid rise of $\langle L_l\rangle$ at higher c_3 values is accompanied by a large increase in the size fluctuations (see Table I), which

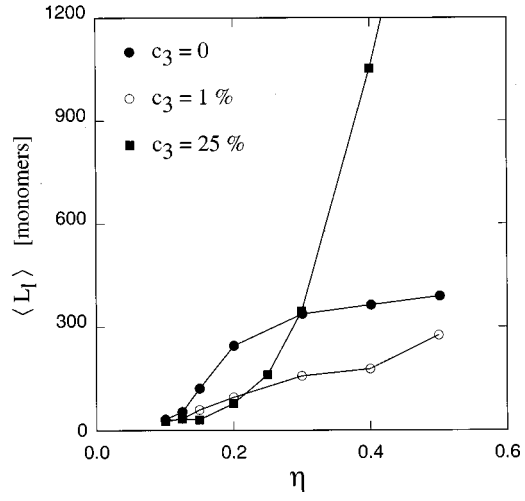

FIG. 9. $\langle L_i\rangle$ as a function of η at three values of c_3. Lines are a guide to the eye.

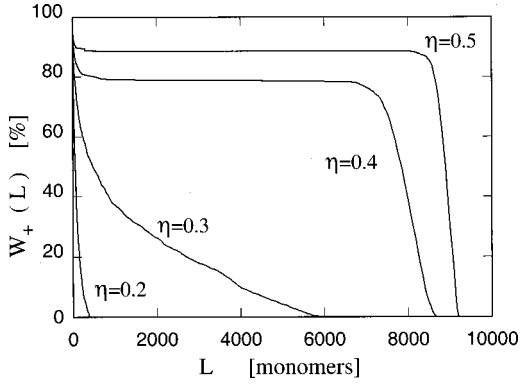

FIG. 10. $W_+(L)$ at four different densities for $c_3=25\%$.

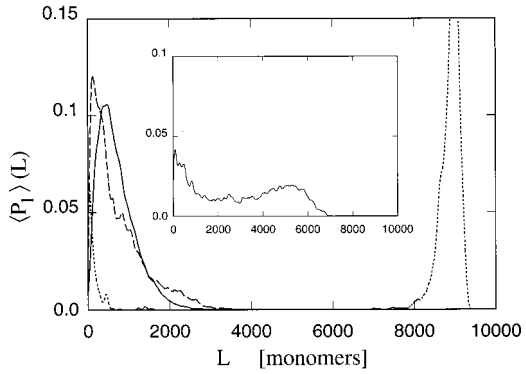

FIG. 11. Mass fraction distribution $\langle P_l \rangle$ in 2D samples at $\eta = 0.5$ and $T = 3$. Full line: $c_3 = 0$; dashed line: $c_3 = 1\%$; dotted line: $c_3 = 25\%$. Inset: $c_3 = 10\%$, corresponding to the gel point.

allows us to locate the gel transition at $c_3 \sim 2\%$ for these conditions of density and T. The same transformations can be observed on the density axis at fixed c_3 (see Fig. 13). As discussed below, the close analogy in the behavior of 2D and 3D systems is confirmed by the analysis of snapshots and of the molecular size distribution $P_l(L)$. The major differences between 2D and 3D results are quantitative: In 3D the relevant density range is reduced by an order of magnitude, the relative reduction of $\langle L_l \rangle$ at low c_3 is much less pronounced and is observed only for $\eta < 0.15$.

At relatively high density ($\eta \geqslant 0.15$), Fig. 13 shows that even a very low value of c_3 ($\sim 0.1\%$) gives rise to a significant enhancement of polymerization ($\langle L_l \rangle$ increases by more than 20% in going from $c_3 = 0$ to $c_3 = 0.1\%$ at $\eta = 0.5$). The criterion used to identify the gel point in 2D systems cannot be used here, since $\langle L_l \rangle (c_3) > \langle L_l \rangle (c_3 = 0)$ at all $c_3 > 0$. However, gelation occurs at these densities ($\eta > 0.15$) at values of c_3 well below 1%, where statistical fluctuations prevent a quantitative determination of the gel point by simulation. On the other hand, neither the polymerization nor the gel transition below the polymerization density $\eta_p(3\mathrm{D})$ for the model without branching were observed up to the highest concentration ($c_3 = 10\%$) studied in 3D.

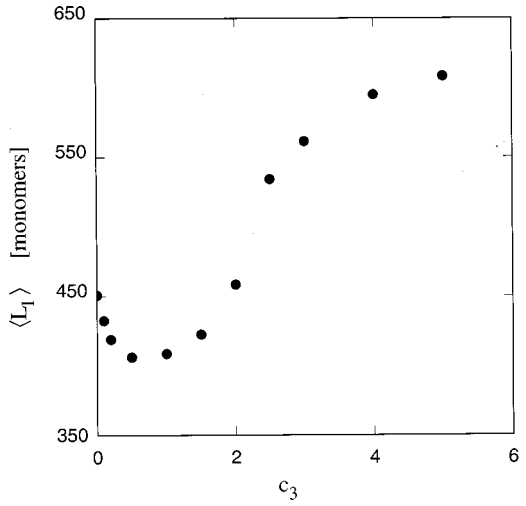

FIG. 12. Average length $\langle L_l \rangle$ of molecules carrying at least one chain termination. Simulations have been performed in 3D, at $T = 3$ and $\eta = 0.05$.

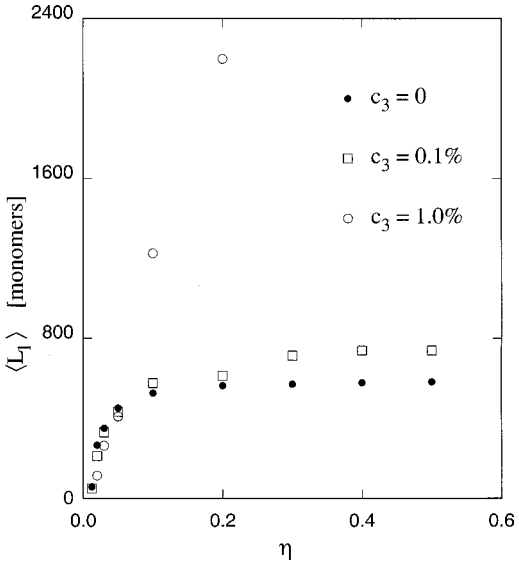

FIG. 13. Average length $\langle L_l \rangle$ of molecules carrying at least one chain termination as a function of η for three values of c_3. Simulations in 3D at $T = 3$.

The dependence of $P_l(L)$ on density and c_3 in 3D samples is greater than that found in 2D, reflecting the increased stability of both polymer and gel. Starting from a $P_l(L) \propto L \exp[-L/\langle L \rangle]$ for $c_3 = 0$, the addition of 0.1%–0.2% of trifunctional particles already changes significantly the shape of $P_l(L)$ (as can be seen in Fig. 14), which is now approximated better by $P_l(L) \propto \exp[-\alpha L/\langle L \rangle]$ ($\alpha \sim 0.3$). With increasing c_3, the height and the width of the first $P_l(L)$ peak decrease monotonically, while the large-L tail develops into a secondary peak at $L \sim 6000$ for $c_3 \sim 1\%$. At the gel point ($c_3 = 2\%$), identified here by the maximum in the relative size fluctuations, $P_l(L)$ is clearly bimodal. For larger values of c_3, most of the weight under the $P_l(L)$

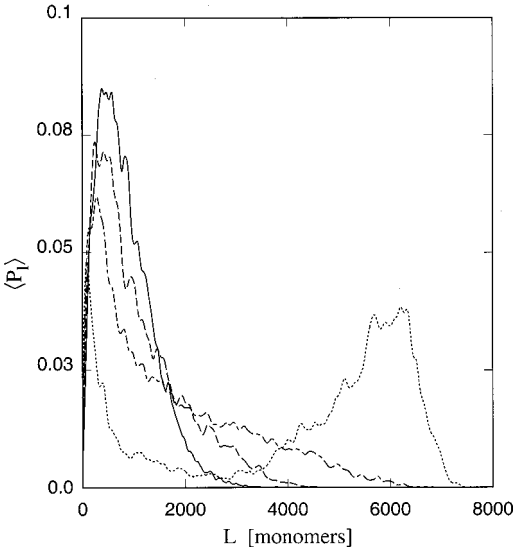

FIG. 14. Mass fraction distribution $\langle P_l \rangle$ in 3D samples at $\eta = 0.05$ and $T = 3$. Full line: $c_3 = 0$; dashed line: $c_3 = 0.2\%$; dot-dashed line: $c_3 = 0.5\%$; dotted line: $c_3 = 2\%$.

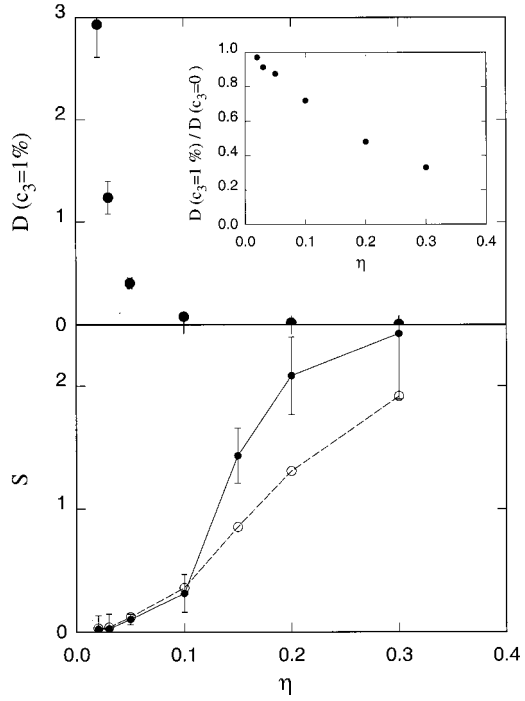

FIG. 15. Lower panel: viscosity coefficient s in 3D samples at $T=3$. Solid dots: $c_3=1\%$; empty circles: $c_3=0$. Upper panel: diffusion coefficient in 3D samples at $T=3$ and $c_3=1\%$. Inset: ratio of the diffusion coefficient at $c_3=1\%$ and at $c_3=0$. Error bars account for statistical errors only. At high density, systematic errors due to long time correlations may exceed the estimated error bar.

curve belongs to the high-L peak, which moves towards larger sizes (saturating at $L\sim 9000$) and reduces its width.

The rapid and significant narrowing of the first P_l peak at low c_3 is consistent with the reduction in the polymerization degree observed in 2D and the systematic reduction of R_g in 3D as c_3 increases. However, the narrowing of the first P_l peak in 3D systems occurs simultaneously with the early formation of the secondary peak at high sizes, resulting in a very limited variation of $\langle L_l \rangle$ at low c_3 concentrations.

The equivalence in the interactions between all particle types means that average structural properties, such as the radial distribution function or the structure factor, are only weakly sensitive to polymerization and gelation, especially at moderately high densities where both transitions are particularly strong. A closer connection between our simulations and experimental measurements could be provided by the analysis of dynamical properties, which we have performed by computing the diffusion and viscosity coefficients. The long relaxation times in polymeric samples mean that it is difficult to obtain converged values for the dynamical coefficients, especially at medium and high density. Nevertheless, our MD trajectories extended up to 3000 time units τ, and the results of Fig. 15 demonstrate the sensitivity of (long time) dynamical properties to branching.

The diffusion coefficient D decreases significantly on introducing even a few branching points ($c_3\sim 1\%$), and the relative effect is stronger at high density (in the gel phase). However, no discontinuity or apparent anomaly in D can be associated to the gel transition. Diffusion in the gel phase is due almost exclusively to the residual population of low molecular weight aggregates, which are also responsible for the low-L peak in the size distribution $P_l(L)$. The relatively high mobility of these species could conceal anomalies in the diffusion of the polymerized fraction, which contributes very little to the average mobility.

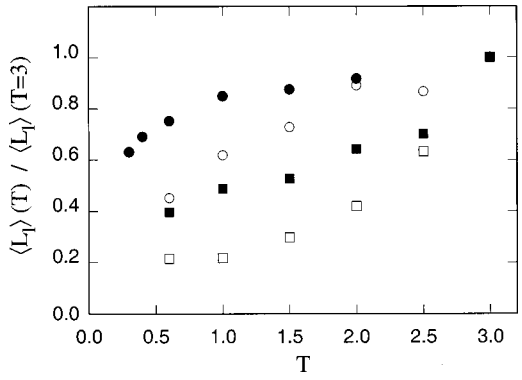

FIG. 16. Ratio of the average length $\langle L_l \rangle$ at temperature T and at temperature $T=3$. Simulations in 2D at $\eta=0.3$. Solid dots: $c_3=0$; empty circles: $c_3=4\%$; solid squares: $c_3=10\%$; empty squares: $c_3=25\%$.

The viscosity coefficient s is a nonmonotonic function of density on the addition of branching points: at low η, the viscosity coefficient initially decreases slightly ($c_3\sim 1\%$), although the decrease is comparable than the statistical error bar, and there is an increase in the viscosity at high density ($\eta \geqslant 0.15$). The crossover between these trends corresponds roughly to the gel transition. Nevertheless, the sensitivity of s to gel formation is weak, and our simulations do not reproduce the dramatic increase of viscosity measured on crossing the gel transition. The slight decrease of viscosity with increasing branching at low density might be due to the compact shape of branched polymeric units, which decreases the intermolecular contributions to viscosity. The weak increase of the viscosity coefficient on going from polymer to gel might reflect the relatively short simulation times. The linking of large polymeric units at branching points manifests itself in long-time correlations for the stress tensor, which enter s the definition of s implemented in our computation,[12] and a detailed description might require much longer simulation times. Nevertheless, the relatively small changes in s on gelation might be due to the coexistence of the gel with a diffuse population of small molecules that prevents a drastic rise of viscosity.

V. DEPENDENCE ON T AND c_a: STRUCTURAL PROPERTIES

The polymerization line of the model results[12,13] from the competition between the translational entropy of small aggregates (dominant at low density) and the entropy of the bonding configuration, which favors large aggregates and is the dominant factor at high density. This role of entropy is emphasized by the T-dependence of polymerization, which becomes weaker with decreasing T. This effect is evident for $c_3=0$ and becomes progressively more important as c_3 increases. This is shown for 2D systems at $\eta=0.3$ in Fig. 16, which shows the T-dependence of the average length $\langle L_l \rangle$ of molecules with chain terminations.

These results are representative of those found for higher densities. At all c_3, polymerization is reduced by lowering T. For high c_3 (see the data for $c_3=25\%$ in Fig. 16), decreasing T from 3 to 0.6 reduces $\langle L_l \rangle$ by an order of magnitude, indicating that the system transforms from gel to polymer. The analysis of snapshots, the mass-fraction distribution $\langle P_l(L) \rangle$, and the molecular size fluctuations all show that the gel characteristics are lost progressively on lowering T. However, the gradual evolution of these properties with changing T prevents the precise determination of the transition point. A more extensive investigation, including a wider range of densities, would be required to characterize the transition better and to fix its boundaries.

The polymerization and gel transitions are slightly less sensitive to temperature in 3D than in 2D, mainly because the relevant range of c_3 is lower. At higher concentrations the negative effect of low T could be as strong as in 2D, although the enhanced stability of large aggregates in 3D could reduce the role of temperature.

The interpretation of gelation as the percolation of a superaggregate formed by linking chains by trifunctional units suggests that c_a might effect the transition significantly. In the absence of branching the average size $\langle L_l \rangle$ scales almost exactly as $1/c_a$, but the relation between c_a and the number of open chains is broken by the presence of branching. Nevertheless, for all c_3, the effect of branching increases with decreasing c_a. This is true both for the reduction in the degree of polymerization at low c_3 (and low density for 3D samples) and for the polymerization enhancement at high c_3, including a stronger tendency towards the gel phase. This observation is consistent with the measurements of Ref. 5, which show that the effects of branching are amplified by decreasing the concentration of the initiator used in the ROP reaction (c_a in our model).

Trifunctional units are uniformly distributed in molecules of all samples (2D and 3D), without apparent segregation at low or high molecular masses. The only significant deviations from the average c_3 value are observed at very low molecular sizes and are due to the topological constraints discussed above.

The origin of the stoichiometry selectivity stabilizing the gel phase at $c_3=25\%$ in 2D requires further study. The 3:1 composition ratio between di- and trifunctional particles indicates enhanced stability for a network of trifunctional particles joined by segments of difunctional particles two monomers long [see Fig. 4(d)]. Analysis of the bonding pattern shows that at $c_3=25\%$ segments of difunctional particles of length two are indeed very common, but the simulations deviate from the ideal motif of Fig. 4(d). The distribution function for the length L_p of polymeric segments comprising difunctional particles is nearly constant for $1 \leqslant L_p \leqslant 3$, and drops almost discontinuously to zero for $\leqslant L_p > 3$. With decreasing c_3, this distribution moves towards higher L_p's and becomes much broader, suggesting that the system gains entropy from a wide distribution in the length of polymeric chains connecting trifunctional particles.

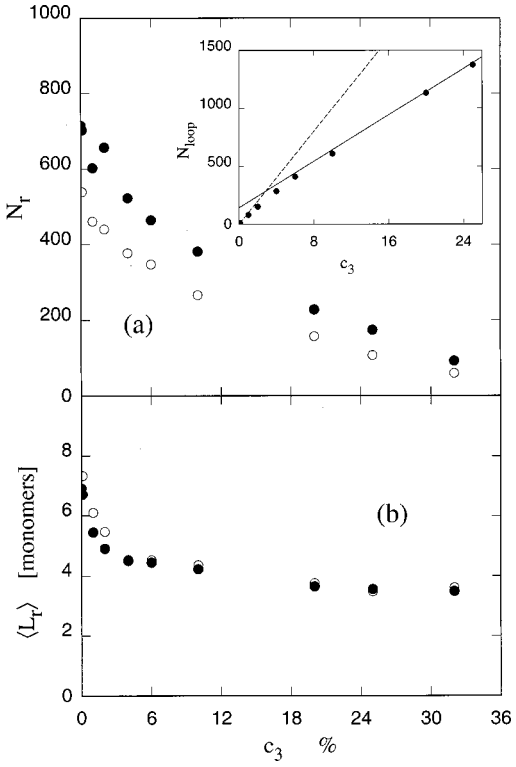

FIG. 17. Average number N_r (a) and average size $\langle L_r \rangle$ (b) of rings in 2D as a function of c_3 at $T=3$. Solid dots: $\eta=0.3$; empty circles: $\eta=0.5$. The lines correspond to the asymptotic behavior $N_{\text{loop}} \sim \alpha + Nc_3/2$ at high c_3, and $N_{\text{loop}} \sim Nc_3$ at low c_3, as discussed in the text.

VI. THE ROLE OF SIMPLE RINGS

Simple rings are the minority component of the polymer in the absence of branching and become progressively less important than open chains as density and dimensionality increase. This picture remains valid when trifunctional units are present, with the additional feature that the average number N_r and the average length $\langle L_r \rangle$ of simple rings decrease monotonically with increasing c_3 (Fig. 17). This is surprising for low c_3 values in 2D, since the lower degree of polymerization would suggest a decreased stability of the competing species, i.e., open chains and other large, complex aggregates.

The decline in the number of simple rings is accompanied by a steady growth of the number N_{loop} of closed polymeric loops belonging to branched molecules (see the inset in Fig. 17). The topological rules of our model do not determine N_r and N_{loop} uniquely, but they set bounds on the latter. As discussed in Sec. II, a molecule with n_3 trifunctional particles has $n_{\text{loop}}=(n_3+2-N_t)/2 \sim (n_3+2)/2$ closed loops.[29] If the number of trifunctional particles in each molecule is low ($n_3 \sim 2-4$ at most), then $n_{\text{loop}}=(n_3+2)/2 \sim n_3$, and $N_{\text{loop}}=\Sigma_{\text{molecules}} n_{\text{loop}} \sim N_3$, or $N_{\text{loop}} \simeq Nc_3$, where N is the total number of monomers. If each molecule contains several trifunctional particles, $n_{\text{loop}} \sim n_3/2$, and $N_{\text{loop}} \simeq \alpha + Nc_3/2$, where the constant α is much smaller than $Nc_3/2$. The representative results of Fig. 17 (for $\eta=0.3$ and $T=3$ in 2D) show that $N_{\text{loop}} \sim Nc_3$ for small c_3, and $N_{\text{loop}} \sim Nc_3/2$ for larger c_3. The crossover is near the point where branching switches from lowering (at low c_3) to enhancing

(at high c_3) the degree of polymerization. The population of closed loops belonging to branched molecules grows rapidly in both regimes, suggesting that closed loops dominate over linear chains and simple rings. The enhanced stability of closed loops underlies the lower degree of polymerization at low c_3 and the gel transition at high c_3.

In the absence of branching, the size distribution function for rings $P_r(L)$ in the polymeric phase displays a pronounced peak at very low sizes ($L\sim 5$), and a low and structureless tail extending up to $L\sim 100$.[13] The decrease in the average size of simple rings $\langle L_r\rangle$ as c_3 increases is due to the disappearance of the large-L tail in $P_r(L)$. With increasing c_3, molecular aggregates of intermediate or large size produced during a reaction are increasingly likely to contain trifunctional units, and they contribute less to the population of simple rings. The resulting $P_r(L)$ become qualitatively similar to those found by previous studies of a model without branching, but with a varying number of bonds determined by thermal equilibrium.[10(b)] The narrow size range covered by $P_r(L)$, together with the low number of rings in samples including trifunctional units (Fig. 17) prevent a more detailed analysis of the analytic behavior of $P_r(L)$ close to the origin.

VII. SUMMARY AND CONCLUDING REMARKS

We have studied the equilibration of a model polymer with LJ particles and a fixed number of harmonic bonds under the influence of *active* particles that promote the interchange of bond pairs. In the absence of branching, the model shows the equilibrium of a high-density polymerized phase and a low-density unpolymerized phase. The addition of trifunctional particles displaces the polymerization line and introduces a qualitatively new gel phase.

The degree of polymerization, as measured by the average molecular sizes $\langle L_l\rangle$, $\langle L_3\rangle$, and $W_+(L)$, is reduced significantly by low concentrations of branching points in 2D samples at all densities. At densities slightly above the polymerization line, the system may revert to the unpolymerized state over a wide range of concentrations c_3 (see the results for $\eta=0.2$ in Fig. 5), since the significant reduction in molecular size (as measured by R_g) strongly enhances the formation of closed loops that limit chain growth. At high density and large values of c_3, the bonding capability of trifunctional particles overcomes the reduction of polymerization. Eventually, the linking of individual molecular units by trifunctional particles gives rise to an aggregate incorporating most of the system mass, and the (continuous) transition is accompanied by anomalous fluctuations in the molecular sizes. These results are consistent with the identification of gelation as a percolative phase transformation, although our simulation goes beyond the assumptions underlying simple analytical descriptions of this transition.

The dramatic changes in the phase diagram are reflected in the evolution of the molecular size distribution, described by the $\langle P_l\rangle$ function (Sec. III). Starting from a Zimm–Schulz distribution $\langle P_l\rangle\propto L^{\gamma}\exp[-\gamma L/\langle L\rangle]$ at $c_3=0$, we observe a reduction in the range of $\langle P_l\rangle$, accompanied by a change to $\langle P_l\rangle\propto\exp[-\alpha L/\langle L\rangle]$ (with $\alpha\sim 0.36$) in the functional form for $\langle P_l\rangle$ that emphasizes the low L portion of the molecular size range. Gelation is identified by a further marked change in $\langle P_l\rangle$, which approaches a very broad step function associated with the large fluctuations in the size distribution that develop at the transition. $\langle P_l\rangle$ becomes markedly bimodal beyond the gel point, with a low-L peak at the origin and a high-L component at sizes approaching the total mass of the simulated samples.

Equilibration is much more difficult to achieve in 3D than in 2D, because polymerization and gelation occur at significantly lower densities, and fluctuations are more important. Nevertheless, most results for 2D systems remain qualitatively valid in 3D. Small concentrations of trivalent particles lower the degree of polymerization at densities $0.04\leqslant\eta\leqslant 0.15$, although this effect is less important than in 3D and is not seen for $\eta\geqslant 0.15$. Relatively high concentrations of trifunctional particles give rise to a continuous transition to the gel phase, which occurs with increasing c_3 and packing fraction η. The evolution of $\langle P_l\rangle$ with increasing c_3 is similar in 2D and 3D. In particular, the first peak of $\langle P_l\rangle$ narrows upon adding trifunctional particles, which parallels the reduction of $\langle L_l\rangle$ at low c_3 found in 2D. The effect on the average size $\langle L_l\rangle$ is partially compensated in 3D systems by the early formation of a secondary peak at large sizes. As a result, the pronounced dip in $\langle L_l\rangle$ seen in 2D at low c_3 is not observed, and size fluctuations indicate more clearly than the average size itself the drastic changes in the molecular population as c_3 increases. The molecular size distribution in 3D is bimodal at the gel point (it was broad and structureless in 2D), suggesting that the order of the transition might be higher than in 2D. However, a detailed discussion of these features would require far more extensive simulations.

The computed diffusion and viscosity coefficients are very sensitive to branching, and low concentrations ($c_3\sim 1\%$) of trifunctional units can be detected by monitoring either. The continuous nature of the transition means that these properties show no marked anomalies at the polymer to gel transition, but the limited simulation times might contribute to this.

Lowering T reduces the degree of polymerization even in the absence of branching, and trifunctional particles enhance greatly the sensitivity to temperature of the polymer and gel phases. The latter is effected more, and we observe a reversible transition between the polymer at low T and the gel at high T, for 2D samples at high density and high values of c_3. The continuous nature of the transition hampers the determination of the transition point in this case. The effect of decreasing T is somewhat reduced in 3D for the (narrow) range of c_3 studied here, although similar effects to those observed in 2D could also occur for larger values of c_3. In both 2D and 3D the enhancement of temperature effects due to branching is consistent with the lower entropy advantage of long chains, which is reflected in the decrease of the degree of polymerization at low c_3.

The changes in the system properties that we observe with changing temperature and density are fully reversible. Moreover, the results described here refer to homogeneous systems. We could not distinguish a network core from a gel boundary, which is sometimes seen in simulations and experiments on highly branched systems,[30] and we found no evidence for long range modulations, such as a prepeak in

the structure factor $S(k)$ at low k. We suggest that the equilibrium condition allows strong inhomogeneities produced by thermal fluctuations to decay, although experiments and computational models for highly branched polymers consider systems in which bond formation is irreversible, and this, too, could lead to inhomogeneous structures.[31]

Simulations have been performed in two and three dimensions over a wide range of stoichiometry and thermodynamic conditions, and the model is appropriate if the intrachain bonds are strong enough to render thermal fluctuations in their number unimportant. This has important consequences for the polymerization transition.[13] The simulations described in Ref. 11 are more restricted in scope and assume a fluctuating number of bonds. Nevertheless, the two studies are closer than many published in recent years. Both show that an increasing number of branching points gives rise to large scale fluctuations and a continuous transition to the gel phase, which is stabilized by increasing density. However, even simulations as extensive as ours (more than two years CPU time) do not cover the entire phase diagram of the model, which presents a fascinating combination of phases and transitions occurring as a function of density, T, and composition.

ACKNOWLEDGMENTS

The calculations were performed in the Forschungszentrum Jülich on a Compaq DS20E server and XP1000 workstations provided in part by the Bundesministerium für Bildung und Wissenschaft, Bonn, within the MaTech-Kompetenzzentrum ''Werkstoffmodellierung'' (03N6015). The authors thank A. Milchev for helpful discussions and correspondence.

[1] G. R. Strobl, *The Physics of Polymers: Concepts for Understanding Their Structures and Behavior* (Springer, Berlin, 1996).
[2] L. Stryer, *Biochemistry*, 4th ed. (Freeman, New York, 1995). A discussion of glycogen is given on p. 587. Branching is an essential feature of this polymer, as it increases its solubility as well as its rate of degradation to glucose 1-phosphate.
[3] Low-density polyethylene produced by free-radical polymerization acquires branching points via a parasitic chain transfer reaction. See P. Ehrlich, Adv. Polym. Sci. **7**, 386 (1970); R. C. M. Zabisky, W.-M. Chan, P. E. Glor, and A. E. Hamielec, Polymer **33**, 2243 (1992); P. Lorenzini, M. Pons, and J. Villermaux, Chem. Eng. Sci. **47**, 3969 (1992).
[4] See, for example, S. M. Clarke, A. Hotta, A. R. Tajbakhsh, and E. M. Terentjev, Phys. Rev. E **64**, 061702 (2001). The anisotropic mechanical behavior of liquid crystal elastomers depends on the way the networks are cross-linked.
[5] H. O. Krabbenhoft and E. P. Boden, Makromol. Chem., Macromol. Symp. **42/43**, 167 (1991). Branching in BPA-PC leads to high heat resistance and high shear sensitivity.
[6] P. G. de Gennes, *Scaling Concepts in Polymer Physics* (Cornell University Press, Ithaca, 1979).
[7] For discussions of these and related topics, see *Kinetics of Aggregation and Gelation*, edited by F. Family and D. P. Landau (North–Holland, Amsterdam, 1984).
[8] For reviews of equilibrium polymerization and related topics, see M. E. Cates and S. J. Candau, J. Phys.: Condens. Matter **2**, 6869 (1990); S. C. Greer, J. Phys. Chem. B **102**, 5413 (1998).
[9] S. C. Greer, Adv. Chem. Phys. **94**, 261 (1996).
[10] Computer simulations studies of equilibrium polymers are reviewed in (a) J. P. Wittmer, P. van der Schoot, A. Milchev, and J. L. Barrat, J. Chem. Phys. **113**, 6992 (2000); (b) A. Milchev, J. P. Wittmer, and D. Landau, Phys. Rev. E **61**, 2959 (2000); (c) J. P. Wittmer, A. Milchev, and M. E. Cates, J. Chem. Phys. **109**, 834 (1998).
[11] See, for example, M. Nosaka, M. Takasu, and K. Katoh, J. Chem. Phys. **115**, 11333 (2001).
[12] P. Ballone and R. O. Jones, J. Chem. Phys. **115**, 3895 (2001).
[13] P. Ballone and R. O. Jones, J. Chem. Phys. **116**, 7724 (2002).
[14] D. J. Brunelle, in *Ring-Opening Polymerization: Mechanisms, Catalysis, Structure, Utility*, edited by D. J. Brunelle (Hanser, München, Germany, 1993), p. 309.
[15] P. J. Flory, J. Am. Chem. Soc. **63**, 3083 (1941); **63**, 3091 (1941); **63**, 3096 (1941).
[16] W. H. Stockmayer, J. Chem. Phys. **11**, 45 (1943).
[17] Most simulation studies of kinetic gelation use the bond fluctuation model of I. Carmesin and K. Kremer, Macromolecules **21**, 2819 (1988); see also E. Del Gado, L. de Arcangelis, and A. Coniglio, Phys. Rev. E **65**, 041803 (2002) for a recent example.
[18] A. Coniglio, H. E. Stanley, and W. Klein, Phys. Rev. Lett. **42**, 518 (1979).
[19] H. J. Herrmann, D. P. Landau, and D. Stauffer, Phys. Rev. Lett. **49**, 412 (1982).
[20] Y. Liu and R. B. Pandey, Phys. Rev. B **55**, 8257 (1997).
[21] M. Vogt and R. Hernandez, J. Chem. Phys. **115**, 1575 (2001).
[22] See, for instance, H. Tobita, J. Polym. Sci., Part B: Polym. Phys. **39**, 2960 (2001); **39**, 391 (2001); R. A. Hutchinson, Macromol. Theory Simul. **10**, 144 (2001).
[23] J. B. Hutchinson and K. S. Anseth, Macromol. Theory Simul. **10**, 600 (2001); H. Tobita, N. Aoyagi, and S. Takamura, Polymer **42**, 7583 (2001).
[24] P. Ballone, B. Montanari, and R. O. Jones, J. Phys. Chem. A **104**, 2793 (2000); see also P. Ballone and R. O. Jones, *ibid.* **105**, 3008 (2001).
[25] The restriction to fixed bonding configurations avoids the discontinuous energy changes that occur on bond interchange. It could be removed by using more sophisticated rules or a different MD algorithm.
[26] D. Stauffer, J. Chem. Soc., Faraday Trans. 2 **72**, 1354 (1976).
[27] O. G. Mouritsen, *Computer Studies of Phase Transitions and Critical Phenomena* (Springer, Berlin, 1994).
[28] L. Schäfer, Phys. Rev. B **46**, 6061 (1992); P. D. Gujrati, *ibid.* **40**, 5140 (1989). In these models the number of chain terminations is not constant, but is determined by thermal equilibrium.
[29] The number of chain terminations N_t is very low and is neglected.
[30] See, for instance, Y. U. Lee, S. S. Jang, and W. H. Jo, Macromol. Theory Simul. **9**, 188 (2000). Another type of inhomogeneous gel phase (microgels) results from the formation of distinct, large molecular aggregates with a high degree of cross-linking. See W. Funke, O. Okay, and B. Joos-Müller, Adv. Polym. Sci. **136**, 139 (1998). Our molecular size distribution $\langle P_l(L)\rangle$ shows, however, that our gel phase contains only one large cross-linked molecule.
[31] Reference 20 discusses the characteristic differences between reversible and irreversible gelation.